Impact of pre-treatments on the surface composition, the optical and flow properties of a CuCrZr powder dedicated to laser powder bed fusion use

Claudia Salvan, Eric de Vito, Laurent Briottet, Thierry Baffie

Impact of pre-treatments on the surface composition, the optical and flow properties of a CuCrZr powder dedicated to laser powder bed fusion use

C. Salvan (Univ. Grenoble Alpes, CEA, LITEN, F-38000 Grenoble, France) claudia.salvan@cea.fr; E. De Vito (Univ. Grenoble Alpes, CEA, LITEN, F-38000 Grenoble, France) eric.de-vito@cea.fr; L. Briottet (Univ. Grenoble Alpes, CEA, LITEN, F-38000 Grenoble, France) laurent.briottet@cea.fr; T. Baffie* (Univ. Grenoble Alpes, CEA, LITEN, F-38000 Grenoble, France) thierry.baffie@cea.fr;
* Corresponding author

Editor version available at: https://doi.org/10.1016/j.powtec.2022.117931

Abstract:

Laser Powder Bed Fusion is not power efficient at processing copper-chromium-zirconium alloy due to the high reflectivity of the powder at the laser standard wavelength (1070 nm). A way to reduce the optical reflectivity is to modify the powder surface. This work aims to study the impact of reduction and oxidation pre-treatments on the surface chemistry of the particles, and to understand their consequences on the powder properties. X-ray photoelectron spectroscopy analyses show that, starting from a 2-3 nm thick native Cu_2O layer, a wet atmosphere leads to the formation of a 54 nm thick Cu_2O layer, whereas a reduction under hydrogen leads to pure copper. Under argon, the Cu_2O thickness slightly increases up to 3-4 nm. The oxidation and the reduction treatments improve the flowability, respectively, by 46 % and 26 %. The reduction increases the reflectivity by 2 %, whereas the oxidation reduces it by 26 %.

Keywords: powder, surface chemistry, CuCrZr alloy, XPS, flowability, reflectivity

1. Introduction

Laser powder bed fusion (L-PBF) is an additive manufacturing process in which a thin layer of a metallic powder is selectively melt using a laser. This step is repeated as many times as necessary to create a 3D object. This process offers the possibility to easily create complex shape objects. This faculty is powerful to build more efficient heat exchangers by enabling the manufacturing complex internal channels [1]. However, processing highly conductive materials, such as pure copper or low-alloyed copper grades, is still challenging with standard 1070 nm infrared lasers, because of the combination of the high optical reflectivity of the powder and of the high thermal diffusivity of the densified material [2].

In the literature, three ways of improving the L-PBF process of pure Cu or low-alloyed copper have been investigated: (i) using a laser with a low wavelength, (ii) working at high power (500 to 1000 W), (iii) modifying the surface of the powder.

The optical absorption of a material is sensitive to the incoming wavelength. At 515 nm, the pure copper and the low-alloyed copper have a higher optical absorption than at 1070 nm [3-4]. At 515nm, Nordet *et al.* [5] show that the optical absorption of a copper powder reaches 75%, which is comparable to the optical absorption of commonly used alloys (such as the 316L or the AlSi12) in the L-PBF process at 1070nm. Density of Cu LPBF parts can reach 99.98% [6].

Working at high power to compensate the amount of energy reflected by the powder. At 500 W and using a 99.99% pure Cu powder, Jadhav *et al.* [7] reached a 99.8% density. However, densities obtained by Colopi *et al.* [8] at 800W, Ikeshoji *et al.* [9] at 1 kW, Imai *et al.* [10] at 800 W and Jadhav *et al.* [11] at 600W were much lower, respectively 99.1%, 96.6%, 96.6% and 98%. Moreover, the use of such a high laser power density combined with the high reflectivity of copper powder can damage the laser optics [11-12].

Recently, some studies have found ways to improve the L-PBF process of pure Cu or low alloyed Cu by a modification of the surface of the powder particles to decrease their optical reflectivity [13]. In the case of pure Cu, Lindström *et al.* [14] and Jadhav *et al.* [15] study the effect of Sn coatings on Cu powders for both increasing optical absorption and forming in-situ alloys. Even with low Sn addition (< 2 wt.%), this method reduces the optical reflectivity of the Cu powder by 40 to 60% and increases the flowability properties of the initial powder by reducing the average avalanche angle of 33% [15]. With a Nickel coating, the Cu reflectivity decreases from 78% to 55-58% at 1070nm [16]. Lassègue *et al.* [17] coated Cu powder with CrZr thanks to physical vapor deposition (PVD) process decreasing by 70% the optical reflectivity compared to Cu powder, and by 68% compared to CuCrZr powder. Using the same idea of a surface modification of the powder, Jadhav *et al.* [18] study the effect of carbon nano-particle addition on Cu powders to increase optical absorption and to create an in-situ de-oxidation of the alloy. A low carbon addition (<0.1 wt.%) reduces the optical reflectivity by 50% and increases the flowability properties of the initial powder. However, fabricated parts showed low electrical and mechanical properties. Using graphene nano-flakes grafted on Cu powder, Tertuliano *et al.* [19] measured a 39% reduction in reflectivity, from 91% to 52%. In the case of low-alloyed Cu, it is also possible to modify the particles surface by enhancing the formation of a nitride or carbide layer. For this purpose, in the case of a Cu-0.89wt.% Cr alloy, Jadhav *et al.* [12] realized a nitrogen heat treatment to form a Cr nitride, which allows forming LPBF parts with 99.1% density. With the same alloy, Jadhav *et al.* [20] grafted carbon nanoparticles and formed a Cr carbide after an argon heat treatment at 750°C. This method reduces the optical reflectivity of the powders from 40% to 50% and improves their flowability [20]. Another possible way to modify the surface of Cu particles is based on oxidation. Jadhav *et al.* [21] study's shows that a thin layer of oxide (105 nm) on Cu particles reduces the optical reflectivity of the powder by 45% at the laser wavelength. Gu *et al.* [22] confirm this 45% reduction after 2 hours under ambient air at either 150°C or 200°C. Moreover, those studies made a link between the diminution of the powder optical reflectivity at the laser beam wavelength and the diminution of the energy density needed to obtain dense parts.

In this study, a gas-atomized low-alloyed Cu alloy, CuCrZr, was used. This kind of powder can be processed efficiently by LPBF in the 300-400W power range ([23-26]) without surface modification of the powder, but a high percentage of the deposited energy is not transferred to the powder bed. In the objective of improving the L-PBF process on this alloy, the oxidation of the powder could be the easiest, cheapest yet scalable solution to treat the powder.

In this paper, the impact of oxidation on a CuCrZr powder has been investigated for the first time. The powder was studied in three different states: after an H_2 heat treatment (reduced powder), after an Ar heat treatment (no or slight oxidization but without contamination) and after an oxidation under humid atmosphere (strong oxidation). The impact of those treatments on the chemical composition of the surface of the particles, as well as on the optical reflectivity and the flowability of the powder, are studied and discussed.

2. Materials and methods

2.1. As-received powder

A spherical 10-45µm (d_{50}=26 µm) gas atomized CuCrZr powder with low quantities of satellites (see Figure 1), fabricated under nitrogen by TLS Technik GmbH & Co, has been used. The composition of the powder, measured by Instrumental Gas Analysis (IGA) and Inductively Coupled Plasma optical emission spectroscopy (ICP-OES), is given in Table 1. The composition conforms to the EN12420:214 standard [27] except for the excessive amount of Fe. The powder is stored under nitrogen to avoid its oxidation.

Element [wt.%]	**Cr**	**Zr**	**Fe**	**Si**	**O**	**Others**	**Cu**
As-received CuCrZr powder	0.751 ± 0.01	0.086 ± 0.002	0.020 ± 0.001	0.005 ± 0.002	0.018 ± 0.002	0.02	*Bal.*
EN12420:2014 standard	0.5-1.2	0.03-0.3	< 0.008	< 0.1	< 0.2		*Bal.*

Table 1 : Chemical composition of as-received CuCrZr powder compared to standard

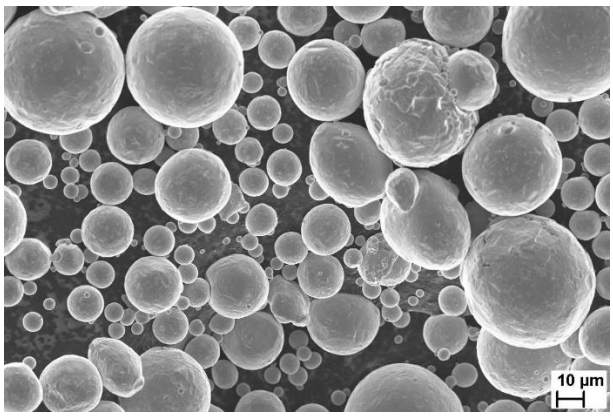

Figure 1 : SEM image of the CuCrZr as-received powder

2.2. Surface modification methods

The as-received CuCrZr powder was treated under three different conditions of atmosphere and temperature (Table 2 to chemically modify its surface: (i) reduction under hydrogen gas (HT-H_2); (ii) a removal of the pollutant at the surface of the particles and a slight oxidation under argon (HT-Ar) and (iii) strong oxidation under high relative humidity (T-97%RH). The heat treatment HT-H_2 was done at 400°C for 4h under 600 mbar of hydrogen in an ELNIK 3002 furnace to reduce the Copper of the CuCrZr alloy. The heat treatment HT-Ar was done at 150°C for 2h in a glovebox under 900 mbar of argon, with partial pressures of O_2 and H_2O maintained below 100 ppmV. Quantity of impurities in Hydrogen and Argon atmospheres were less than or equal to, respectively, 0.005 vol.% and 0.002 vol.%. The treatment T-97%RH consisted in keeping the powder under a 97% relative humidity (RH) atmosphere for 150 days at 25°C. After the treatments, the powders were stored in a glove box under argon atmosphere for a minimum period of time before their transfer to the analysis equipment.

Powder Name	**Temperature [°C]**	**Time**	**Atmosphere**
HT-H_2	400	4 h	600 mbar - Hydrogen
HT-Ar	150	2 h	900 mbar - Argon
T-97%RH	25	150 days	97% RH

Table 2 : Treatments used to modify the surface of the as-received CuCrZr powder

2.3. Characterization of the as-received and surface-modified CuCrZr powders

X-ray photoelectron spectroscopy (XPS) analyses was used (i) to characterize the chemical environments existing at the surface of the powders, and to estimate their surface elemental composition before and after the treatments, (ii) to estimate the thickness of the oxidized layer on the surface.

The powders were transferred from the argon storage glove box to the XPS by a hermetic chamber. Analyses were performed on an XPS Versaprobe II (Physical Electronics) with a 15 keV beam and a pass energy of 23.5 eV (corresponding to an energy resolution of ~0.6 eV). The estimation of the thickness of the oxidized layer was determined by achieving a profile concentration measurement. Ion gun etch cycles were performed by using an Ar^+ ion beam at 0.5 keV energy with a current density of 2.5 $\mu A.cm^{-2}$. The estimated sputtering rate is estimated at 22 $Å.min^{-1}$ [28].

The flowability of the different powders was estimated by the calculation of the Hausner ratio and the measure of the avalanche angle. The Hausner ratio is defined by the equation (1) [29].

$$I_{Hausner} = \frac{V_{apparent}}{V_{tapped}} \quad (1)$$

The apparent volume ($V_{apparent}$) is the volume of the freely settled powder and the tapped volume (V_{tapped}) is the volume of the same amount of powder obtained after 10 000 taps. This measure was done on a J. Engelsmann AG tap density equipment using a 100 mL cruet. The initial volume of the powder was 100 mL except for the T-97%RH powder, for which only 65 mL was used. The analysis was made in a glove box to control the oxygen and water contents in the atmosphere below 100 ppmV max each.

The avalanche angle is the median angle obtained from the image analysis of 150 avalanche angles recorded by a camera. This measurement was made on a Mercury Scientific Revolution® powder analyzer. The drum used is hermetic and is filled with 80 mL of powder in a glove box (partial pressures of O_2 and H_2O maintained below 100 ppmV). The speed rotation rate was 0.3 rotation per minutes.

The optical reflectivity of the powders was analyzed by spectrophotometry between 250 and 1500 nm wavelengths thanks to a LAMBDA 950 PerkinElmer laser spectrophotometer. Powders were placed in 3500 µL quartz cells of 12.5 x 12.5 x 46 mm external dimensions.

3. Results

3.1. Analysis of the powder surface chemical composition

The presence of metallic Cu, cuprous oxide Cu_2O and cupric oxide CuO can be identified by combining the analysis of the Cu $2p_{3/2}$ XPS spectrum and the determination of the kinetic energy position of Cu $L_3M_{45}M_{45}$ Auger transition and drawing the Cu LMM Wagner plot ([30-31] (Figure 2)).

The surface of the as-received powder particles is mainly composed of Cu_2O. The Cu $2p_{3/2}$ spectrum can be resolved in two peaks, located at 932.5 eV and 933.9 eV respectively. The relative positions of the peak at 932.5 eV and of the Cu $L_3M_{45}M_{45}$ Auger transition at 917.1 eV, reported on the Cu LMM Wagner plot, allow confirming the presence of Cu_2O at the surface of the as-received powder [32]. Moreover, the peak at 933.9 eV in the Cu $2p_{3/2}$ spectrum is characteristic of the presence of copper carbonate $CuCO_3$ [33] or copper hydroxide $Cu(OH)_2$ [34]. The sputter profile shows that the oxide layer thickness at the surface of the particle is lower than 3 nm. In fact,

at the end of the concentration profile, the main Cu $L_3M_{45}M_{45}$ peak vanishes and is progressively replaced by a peak at 918.9 eV, characteristic of metallic Cu.

The surface of the HT-H_2 particles is composed of metallic Cu, as shown by the relative positions of Cu $2p_{3/2}$ XPS peak and Cu $L_3M_{45}M_{45}$ Auger transition peak (respectively at 932.7 eV and 918.6 eV). The treatment has thus efficiently reduced the cuprous oxide layer originally present at the surface of the as-received powder.

The surface of the HT-Ar particles is similar to that of the as-received powder. Indeed, it is also composed of Cu_2O as shown by the position of the Cu $2p_{3/2}$ and Cu $L_3M_{45}M_{45}$ peaks (respectively at 932.5 eV and 918.8 eV). The only difference concerns the oxide layer thickness which is slightly higher, as the shift in the main peak (from 918.8eV to 916.8eV) occurs at a depth of 3 to 4 nm. This confirms the effect of the slight oxidation desire with this treatment and is in accordance with the Wagner diagram (Figure 2 (c)).

The Cu $2p_{3/2}$ XPS spectrum of the T97%RH powder reveals satellites peaks located in the 939-944 eV binding energy range and a main peak which can be resolved into three contributions at 932.5, 933.7 and 935.1 eV. The presence of the satellite peaks, the position of the main contribution in the Cu $2p_{3/2}$ XPS spectrum (933.7eV) and the position of the Auger transition peak Cu $L_3M_{45}M_{45}$ 917.8eV (kinetic energy) reveal, thanks to the Wagner plot, the presence of CuO at the surface of the particles. The presence of the smaller contribution at 932.5 eV can also indicate low amounts of Cu_2O. Furthermore, the 935.1 eV contribution is characteristic of the presence of $Cu(OH)_2$ and/or $CuCO_3$. With Ar^+ sputtering, the Cu $2p_{3/2}$ satellite peaks decrease and the major contribution shifts from 933.7 eV to 932.5eV, while the Cu $L_3M_{45}M_{45}$ peak shifts to a lower kinetic energy (916.8eV after sputtering 54 nm). The ion beam preferentially removes the Cu atoms [35]; yet, an oxygen depletion is observed with the successive sputtering steps, which confirms the stronger presence of Cu_2O through the abrasion with a gradual transition from CuO to Cu_2O. After the "54 nm" sputtering step, a small peak appears at 918.5eV on the Cu $L_3M_{45}M_{45}$ Auger transition: this can be related to metallic Cu due to the removal of the oxide layer in some parts at the surface of the particles.

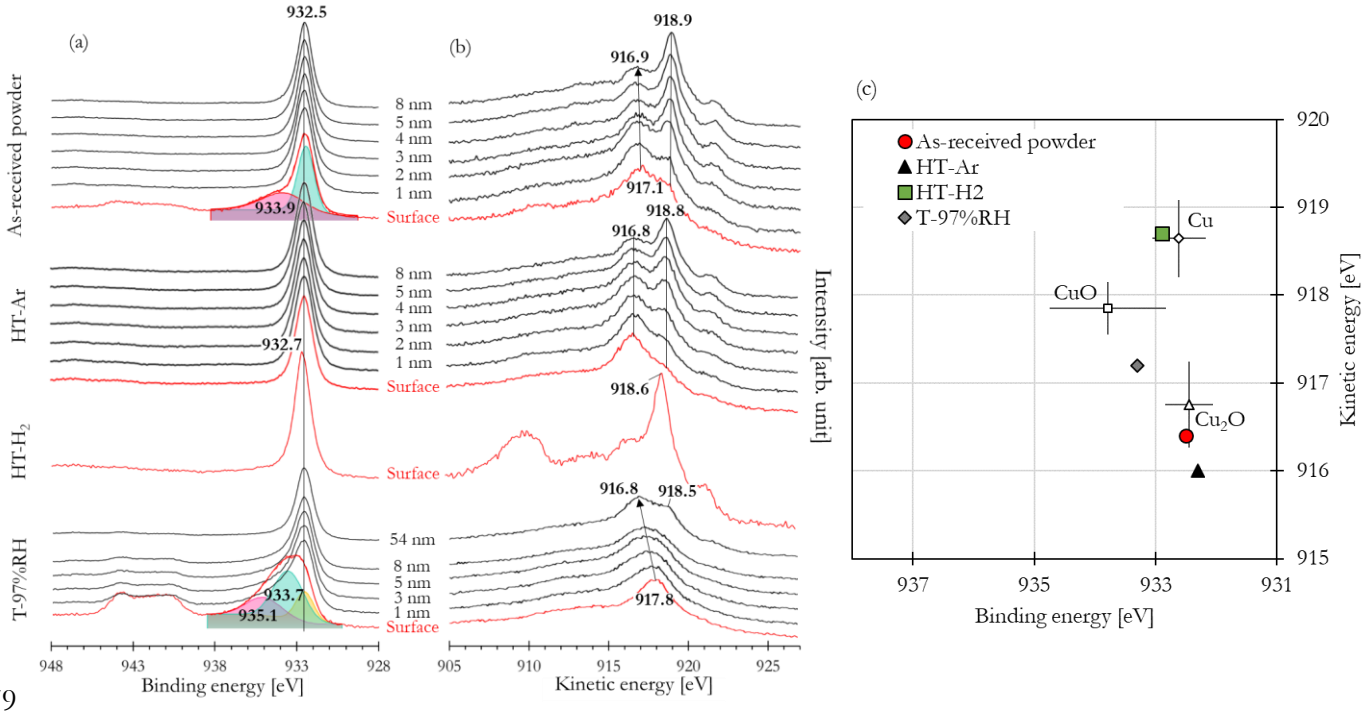

Figure 2 : (a) Cu $2p_{3/2}$ and (b) Cu $L_3M_{45}M_{45}$ XPS spectra at the surface and after several etching cycles for the different studied powders and (c) the Cu LMM Wagner plot at the surface of the particles.

However, other elements and compounds are detected. Hence, Figure 3 presents the Zr $3d_{5/2}$, Cr 3p, C 1s and O 1s XPS spectra recorded together with Cu 2p spectra presented above.

The position of the more intense Zr $3d_{5/2}$ peak, observed for all powders in the 181.8-182.5 eV range (Figure 3 (a, e, i, m)) reveals the presence of ZrO_2 [30,31,36]. For the as-received powder and HT-Ar powder, a less intense peak can be detected at 179.0 and 179.1 eV. This peak can be due to metallic Zr or to ZrO_2 [30]. However, the tendency of metallic Zr to form oxides, due to its high sensitivity to oxygen-rich atmospheres (typically at ambient air), favours the ZrO_2 hypothesis.

The position of the Cr 3p peak, also observed on all powders in the 43.4-44.0 eV range, (Figure 3 (b, f, j, m)) reveals the presence of Cr_2O_3 at the surface of the particles [37–39].

The peak on the C 1s spectrum located at 284.8 eV, also detected for all powders, is characteristic of the C-C/C-H bonds. The green peaks on these spectra (between 288.7 and 288.9 eV, Figure 3 (c, g, o)) is attributed to $CuCO_3$ in relation with the 935.1 eV peaks in the Cu 2p3 spectra, even if the peak position is not totally in accordance with the literature (289.1 eV according to [33]). However, this peak is less intense in the HT-Ar powder than on the as-received powder. In particular, the C 1s intensity ratio is 3.3 for the HT-Ar powder versus 8.3 for the as-received powder. This suggests that the heat treatment decreases the quantity of $CuCO_3$ at the surface of the particles. Finally, other peaks are detected around 286 eV in the as-received and HT-Ar powders (Figure 3 (c, g)). They have not been clearly identified though they may be related to some external contamination.

The O 1s spectrum can also be resolved into different peaks. In the as-received powder (Figure 3 (d)), the 530.0 eV peak is characteristic of metal oxides presence [30] such as Cr_2O_3, ZrO_2 or Cu_2O. The 531.3 eV peak reveals the presence of metallic carbonate such as $CuCO_3$ or a hydroxide such as $Cu(OH)_2$. The highest binding energy peak, located at 532.0 eV, is associated with the presence of surface contamination. After argon or hydrogen-based heat treatment, the O 1s XPS spectra are

highly modified (Figure 3 (h, l)). The carbonate/hydroxide related peaks disappear. The 530.3 eV and 530.5 eV peaks remain, indicating the presence of metal oxides, and the high-energy peaks at 531.7 and 532.0 eV are still associated with surface contamination. In the T-97%RH powder, CuO (529.5 eV) and other metal oxides (530.9 eV) together with a surface contamination (531.7 eV) are observed.

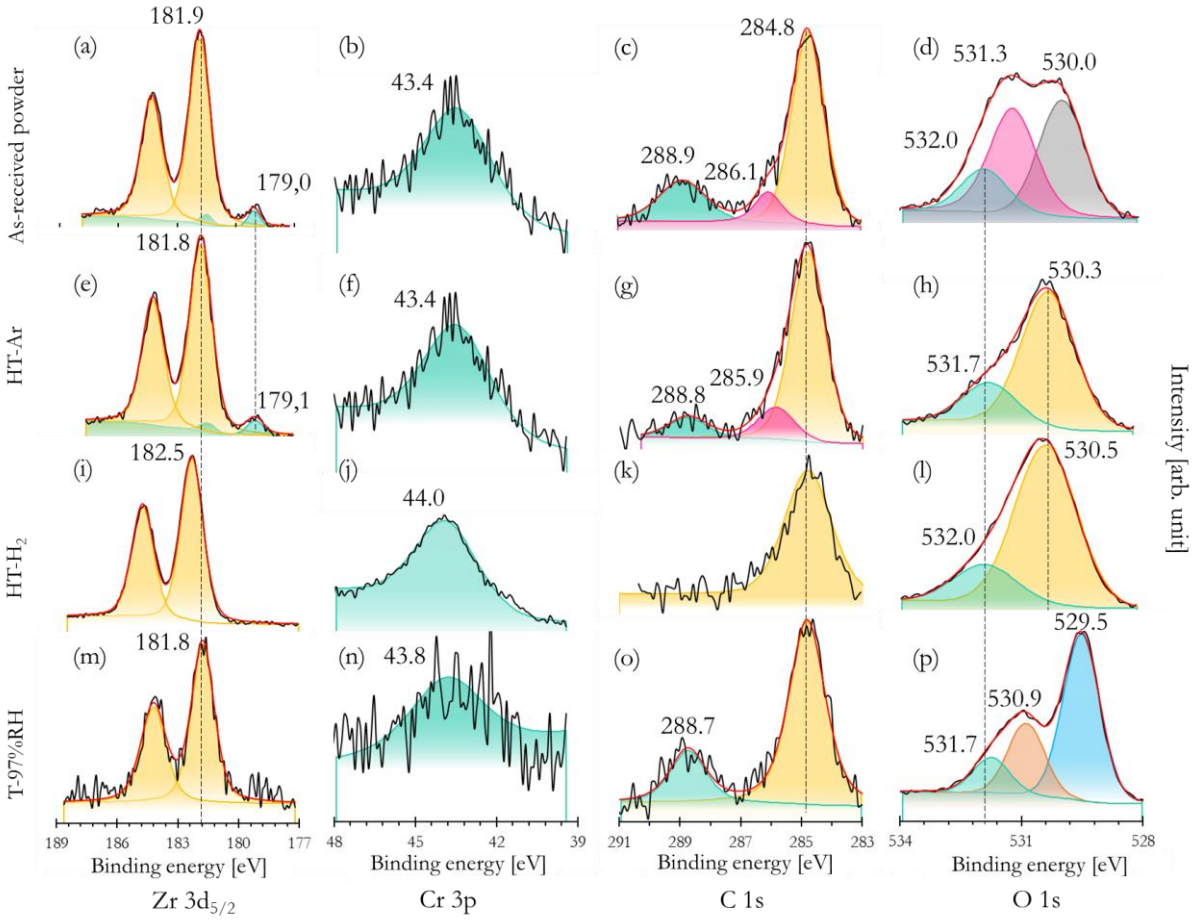

Figure 3 : (a, e, i, m) Zr $3d_{5/2}$, (b, f, j, n) Cr 3p, (c, g, k, o) C 1s, (d, h, l, p) O 1s XPS spectra of the (a-d) as-received powder, (e-h) HT-Ar powder, (i-l) HT-H_2 powder and (m-p) T-97%RH powder.

The species identified at the surface of the CuCrZr powders depending on the heat treatments are summarized in Figure 6.

3.2. Effect of the heat treatments on the powder optical reflectivity

The different applied treatments have an impact on the optical reflectivity at the wavelength of the laser as shown in Figure 4. Initially, the as-received powder had an optical reflectivity of 57 ± 1% at 1070 nm. The hydrogen treatment (HT-H_2) slightly raises the optical reflectivity to 59 ± 1%, whereas the argon treatment (HT-Ar) and the humid atmosphere treatment (T-97%RH) tend to decrease the optical reflectivity to a minimum of 31 ± 1%. The optical reflectivity is the highest when copper oxides are reduced with the HT-H_2 treatment, and decreases with thickness increase of the oxide layer.

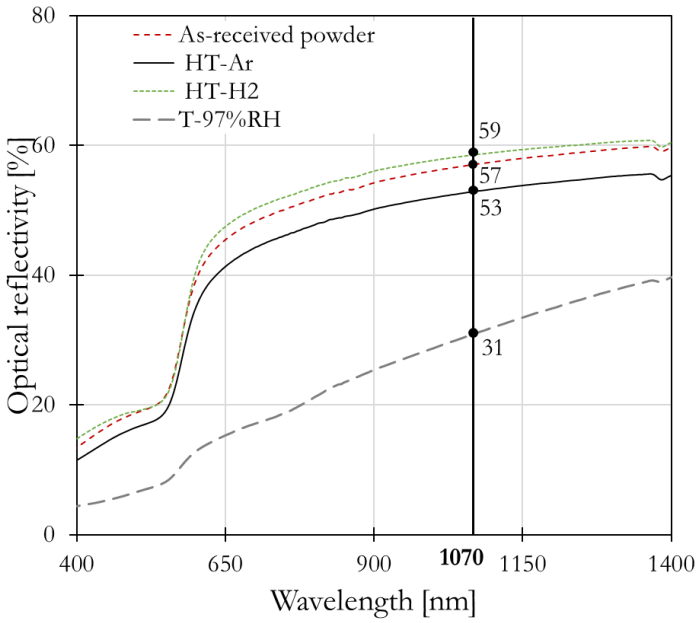

Figure 4 : Optical reflectivity of the CuCrZr powders after different treatments, measured by spectrophotometry

3.3. Flowability

3.3.1. Hausner ratio

In order to investigate the evolution of the CuCrZr powder flowability after the various treatments investigated, the Hausner ratio is calculated (Table 3). The HT-Ar treatment does not change the flowability of the powder as the Hausner ratio does not significantly change after the treatment. By contrast, the hydrogen and the humid atmosphere treatments reduce the Hausner ratio, improving flowability.

CuCrZr powders	$V_{apparent}$ **[mL]**	V_{tapped} **[mL]**	$I_{Hausner}$
As-received powder	100	86	1.16 ± 0.01
HT-Ar powder	100	85.2	1.17 ± 0.01
HT-H_2 powder	100	89	1.12 ± 0.01
T-97%RH powder	65	58.5	1.11 ± 0.02

Table 3 : Apparent volume, tapped volume and Hausner ratio of the different CuCrZr powders

3.3.2. Avalanche angle

The measured avalanche angles (Figure 5) of the different powders confirm that the treatments made on the as-received powder may alter its flowability. The as-received powder has poor flowability as the high median avalanche angle (59°) shows. The argon heat treatment has no effect on the avalanche angle. By contrast, the hydrogen heat treatment reduces significantly the mean avalanche angle (44°). This confirms the trend observed on the Hausner ratio: this treatment increases the flowability of the powder. However, the distribution of the angles is scattered which indicates an irregular flow as for the as-received and the HT-Ar powders. The T-97%RH treatment offers the lower mean avalanche angle (32°) and the narrower distribution, resulting in an easier and smoother flow.

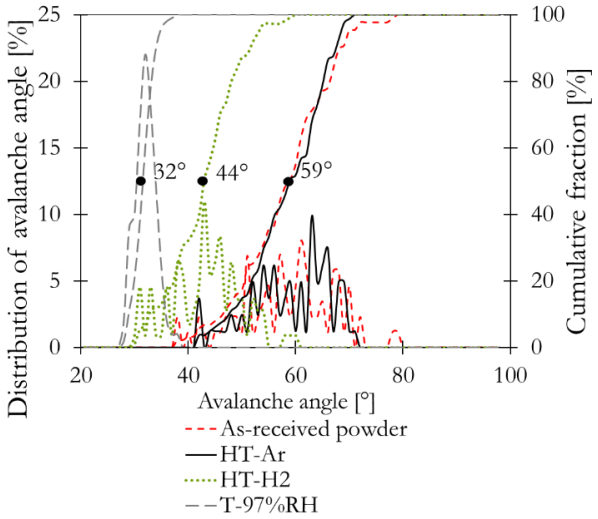

Figure 5 : Distribution and cumulative fraction curves of the avalanche angles (the 32°, 44° and 59° are the mean avalanche angle of the curves)

Two of these powders were tested in three different L-PBF machines: a ProX200 (3D Systems, USA), a FS271 (Farsoon, China) and a SLM125 (SLM Solutions, Germany). For the two first, powder was delivered by a feed tray whereas, for the third one, powder was delivered by a gravity dispenser. The flowabilities of the as-received and the HT-Ar powders were good enough to be used on the ProX200 and the FS271 equipment, but not good enough to be used on the SLM125 equipment.

3.4 Synthesis

Results show that the surface of the as-received powder is composed of a thin layer of Cu_2O (2-3 nm). After HT-Ar, the layer grows to 3-4 nm and after a T-97%RH, the oxidized part of the particles is composed at the top surface of a thin layer of CuO (1 to 2 nm) below a thick layer of Cu_2O (>54 nm). A HT- H_2 reduces entirely the copper. The presence of Cr_2O_3 and ZrO_2 is always detected in the measurements (Figure 6). Finally, the optical reflectivity and the flowability of the powder vary depending on the treatment applied (Figure 6).

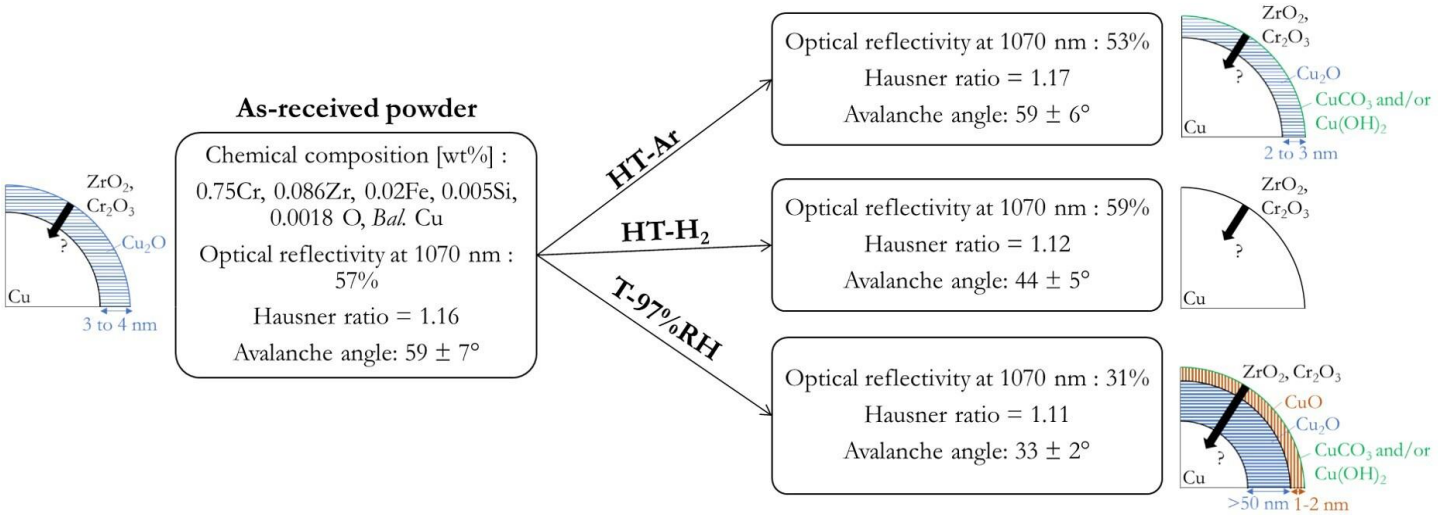

Figure 6 : Summary of the chemical species identified by XPS at the surface of the particles. The corresponding optical reflectivity, Hausner ratio and avalanche angle for the as-received and surface modified CuCrZr powders are also reported.

4. Discussion

4.1. Link between treatment and oxygen content

The presence of the oxidized layer for the copper particles may have an impact on the oxygen concentration in the overall CuCrZr powder. The oxygen content in the as-received powder is 18 wppm, for a Cu_2O layer thickness of 2 to 3 nm. Jadhav *et al.* [21] measured the oxygen content of an oxidized Cu powder with a d_{50}=45 µm covered with a 100 nm layer (mixture of Cu_2O and CuO oxides), close to our T-97%RH, and found an oxygen content of 2000 wppm. These results show that it is possible to control the oxidized layer thickness of a CuCrZr powder from 2 nm to more than 54 nm, by applying treatments on the powder, but this will increase the total oxygen content. Moreover, increasing the oxidized layer thickness may have a positive impact on the LPBF components mechanical properties. Jadhav et al. [21] indicate that the oxygen picked up by a Cu powder during the oxidation stage remains in the as-built part. With a Cu powder having an oxygen content of 2000 wppm, they showed that LPBF parts produced in Argon and in Nitrogen present oxygen contents of, respectively, 2100 wppm and 2200 wppm. They measured a 43% hardness increase of LPBF oxidized Cu parts compared to the ones made of pure Cu powder without affecting the electrical properties [21]. In the case of CuCrZr, a higher oxygen content in the powder would have the same effect. Oxygen will remain trapped in the matrix forming nanometric precipitates and thus an oxide-reinforced material. Indeed, this formation is due to the low oxygen solubility in the copper matrix [40].

4.2. Loss of optical reflectivity

The oxide layer at the surface of the particles also modifies the optical reflectivity. The optical absorptivity (A) and the optical penetration (δp) of an electromagnetic radiation can be defined thanks to equations (2) and (3) [41] [12]:

$$A = 1 - R = \frac{4n}{(n+1)^2 + k^2} \quad (2)$$

$$\delta p = \frac{\lambda}{4\pi k} \quad (3)$$

With R the optical reflectivity, n the refractive index, k the extinction coefficient, λ the wavelength of the electromagnetic radiation [nm]. The data used for this calculation are reported in Table 4.

	$\lambda\ [nm]$	n	k	A	$\delta p\ [nm]$
Cu_2O	1086,4	2,59	0,035	0,80	2505
CuO	1086,4	2,62	0,001	0,80	71808
Cu	1083,3	0,36	7,147	0,03	12

Table 4 : optical absorptivity and optical penetration calculated for the different elements [42].

A powder with the presence of metallic Cu at its surface, without any oxide layer (case of HT-H_2 powder) will have a low optical absorptivity and a small optical penetration. At the opposite, an infinite layer of Cu oxide will have a high optical absorptivity and a high optical penetration. The resulting low reflectivity is a way to improve the transfer of laser energy to the powder bed. In the case of the CuCrZr powders studied in the present paper, the thicknesses of the oxide layers are not infinite, and are just 2 to 4 nm thick in the case of the as-received powder and the HT-Ar powder and correspond to an intermediate case. The penetration of the laser in the Cu_xO is more important than the layer thickness of oxide (Table 4), and then the laser will interact with the Cu_xO/Cu interface inducing multiple optical reflections [43] which are less efficient in reducing the optical reflectivity. This is why a thick layer of surface oxides, at least equal to 50 nm, is needed

to obtain a low optical reflectivity at the L-PBF laser wavelength (1070 nm). However, a thick layer of copper oxide leads to a high oxygen content in the powder, which may have a significant impact on the produced parts. Thus, a compromise has to be found between these parameters.

5. Conclusions

In this paper, the impact of different treatments on the nature of the surface components of a CuCrZr powder has been addressed. Their consequences on the flowability and optical reflectivity of the powder, which are key properties for the L-PBF process, have been discussed.

It has been shown that the presence of an oxide layer and its thickness can be controlled by applying different treatments. The as-received powder is composed of a thin (2 to 3 nm) Cu_2O layer including Cr_2O_3 and ZrO_2 presence. Applying a hydrogen heat treatment fully reduces the copper but have no effect on the oxidized Cr and Zr elements. A heat treatment under argon slightly increases the Cu_2O oxide layer (3 to 4 nm) originally present at the surface of the particles. Leaving the powder under a humid atmosphere has a strong impact on the oxidation of the powders by strongly increasing the thickness of the oxidized layer Cu_2O at the top of the powder to at least 54 nm and by creating a thin 1 to 2 nm layer of CuO at the top of the particles.

It have been proven that the treatments apply on the powder have an impact on its flowability. The as-received and HT-Ar powders have the poorer flowability (avalanche angle of 59°); applying a reducing heat treatment (HT-H_2) increases the flowability properties of the powder (avalanche angle of 44°) even is the flow is still irregular; an oxidation treatment (T-97%RH) has the best impact on the flowability properties on the powder (avalanche angle of 32°).

The treatments applied on the powder also have an impact on its optical reflectivity. The maximum optical reflectivity is obtained after the HT-H_2 reduction (59%) and the minimum optical reflectivity is obtained after the T-97%RH oxidation (31%). Yet, a correlation may be done between the oxide layer thickness and the optical reflectivity of the powder.

Additional work would be necessary to improve the treatments in order to get a fine control of the oxide layer thickness and its composition. Processing these different CuCrZr powders by L-PBF is still to be studied in order to understand the impact of the different treatment on the chemical and physical properties of the parts.

Acknowledgement

The authors gratefully acknowledge CEA-LITEN and the CARNOT "Energies du Futur" program for their financial support. The XPS measurements were performed at the CEA NanoCharacterization Platform (PFNC) - Minatec, supported by the French RTB (IRT Nanoelec) and the equipex NanoIDT.

References

[1] Z. Ma, K. Zhang, Z. Ren, D.Z. Zhang, G. Tao, H. Xu, Selective laser melting of Cu–Cr–Zr copper alloy: Parameter optimization, microstructure and mechanical properties, J. Alloys Compd. 828 (2020). https://doi.org/10.1016/j.jallcom.2020.154350.

[2] M. Colopi, L.Caprio , A.G. Demir, B. Previtali, Selective laser melting of pure Cu with a 1 kW single mode fiber laser, Procedia CIRP Volume 74, 2018, Pages 59-63. https://doi.org/10.1016/j.procir.2018.08.030.

[3] N. Tissot, Amélioration du procédé LBM par nanostructuration de poudres d'aluminium, PhD Thesis, ENI St Etienne, 2019.

[4] A.G. Demir, M. Colopi, B. Previtali, The use of a ns-pulsed, high repetition rate green laser for SLM of 99.9% pure Cu, Lasers in Manufacturing Conference 2019, Munich, Germany, 2019: p. 8. http://hdl.handle.net/11311/1121209.
[5] G. Nordet, C. Gorny, Y. Mayi, J. Daligault, M. Dal, A. Effernelli, E. Blanchet, F. Coste, P. Peyre, Absorptivity measurements during laser powder bed fusion of pure copper with a 1 kW cw green laser, Opt. Laser Technol. 147 (2022) 107612. https://doi.org/10.1016/j.optlastec.2021.107612.
[6] S. Gruber, L. Stepien, E. López, F. Brueckner, C. Leyens, Physical and Geometrical Properties of Additively Manufactured Pure Copper Samples Using a Green Laser Source, Materials. 14 (2021) 3642. https://doi.org/10.3390/ma14133642.
[7] S.D. Jadhav, L.R. Goossens, Y. Kinds, B.V. Hooreweder, K. Vanmeensel, Laser-based powder bed fusion additive manufacturing of pure copper, Addit. Manuf. 42 (2021) 101990. https://doi.org/10.1016/j.addma.2021.101990.
[8] M. Colopi, A.G. Demir, L. Caprio, B. Previtali, Limits and solutions in processing pure Cu via selective laser melting using a high-power single-mode fiber laser, Int. J. Adv. Manuf. Technol. 104 (2019) 2473–2486. https://doi.org/10.1007/s00170-019-04015-3.
[9] T.-T. Ikeshoji, K. Nakamura, M. Yonehara, K. Imai, H. Kyogoku, Selective Laser Melting of Pure Copper, JOM. 70 (2018) 396–400. https://doi.org/10.1007/s11837-017-2695-x.
[10] K. Imai, T.-T. Ikeshoji, Y. Sugitani, H. Kyogoku, Densification of pure copper by selective laser melting process, Mech. Eng. J. 7 (2020) 19-00272-19–00272. https://doi.org/10.1299/mej.19-00272.
[11] S.D. Jadhav, S. Dadbakhsh, L. Goossens, J.-P. Kruth, J. Van Humbeeck, K. Vanmeensel, Influence of selective laser melting process parameters on texture evolution in pure copper, J. Mater. Process. Technol. 270 (2019) 47–58. https://doi.org/10.1016/j.jmatprotec.2019.02.022.
[12] S.D. Jadhav, P.P. Dhekne, S. Dadbakhsh, J.-P. Kruth, J. Van Humbeeck, K. Vanmeensel, Surface Modified Copper Alloy Powder for Reliable Laser-based Additive Manufacturing, Addit. Manuf. 35 (2020) 101418. https://doi.org/10.1016/j.addma.2020.101418.
[13] R. Bidulsky, F.S. Gobber, J. Bidulska, M. Ceroni, T. Kvackaj, M.A. Grande, Coated Metal Powders for Laser Powder Bed Fusion (L-PBF) Processing: A Review, Metals. 11 (2021) 1831. https://doi.org/10.3390/met11111831.
[14] V. Lindström, O. Liashenko, K. Zweiacker, S. Derevianko, V. Morozovych, Y. Lyashenko, C. Leinenbach, Laser Powder Bed Fusion of Metal Coated Copper Powders, Materials. 13 (2020) 3493. https://doi.org/10.3390/ma13163493.
[15] S.D. Jadhav, D. Fu, M. Deprez, K. Ramharter, D. Willems, B. Van Hooreweder, K. Vanmeensel, Highly conductive and strong CuSn0.3 alloy processed via laser powder bed fusion starting from a tin-coated copper powder, Addit. Manuf. 36 (2020) 101607. https://doi.org/10.1016/j.addma.2020.101607.
[16] R. Zheng, J. Cui, Y. Yang, S. Li, R.D.K. Misra, K. Kondoh, Q. Zhu, Y. Lu, X. Li, Enhanced densification of copper during laser powder bed fusion through powder surface alloying, J. Mater. Process. Technol. 305 (2022) 117575. https://doi.org/10.1016/j.jmatprotec.2022.117575.
[17] P. Lassègue, C. Salvan, E. De Vito, R. Soulas, M. Herbin, A. Hemberg, T. Godfroid, T. Baffie, G. Roux, Laser powder bed fusion (L-PBF) of Cu and CuCrZr parts: Influence of an absorptive physical vapor deposition (PVD) coating on the printing process, Addit. Manuf. 39 (2021) 101888. https://doi.org/10.1016/j.addma.2021.101888.
[18] S.D. Jadhav, S. Dadbakhsh, J. Vleugels, J. Hofkens, P. Van Puyvelde, S. Yang, J.-P. Kruth, J. Van Humbeeck, K. Vanmeensel, Influence of Carbon Nanoparticle Addition (and Impurities) on Selective Laser Melting of Pure Copper, Materials. 12 (2019) 2469. https://doi.org/10.3390/ma12152469.

[19] O.A. Tertuliano, P.J. DePond, D. Doan, M.J. Matthews, X.W. Gu, W. Cai, A.J. Lew, Nanoparticle-enhanced absorptivity of copper during laser powder bed fusion, Addit. Manuf. 51 (2022) 102562. https://doi.org/10.1016/j.addma.2021.102562.
[20] S.D. Jadhav, P.P. Dhekne, E. Brodu, B. Van Hooreweder, S. Dadbakhsh, J.-P. Kruth, J. Van Humbeeck, K. Vanmeensel, Laser powder bed fusion additive manufacturing of highly conductive parts made of optically absorptive carburized CuCr1 powder, Mater. Des. 198 (2021) 109369. https://doi.org/10.1016/j.matdes.2020.109369.
[21] S.D. Jadhav, J. Vleugels, J. Kruth, J. Van Humbeeck, K. Vanmeensel, Mechanical and electrical properties of selective laser-melted parts produced from surface-oxidized copper powder, Mater. Des. Process. Commun. 2 (2019). https://doi.org/10.1002/mdp2.94.
[22] R.N. Gu, P. Chen, Y.H. Zhou, H. Wang, X.C. Yan, K.S. Wong, M. Yan, Intentional Oxidation and Laser Remelting of Highly Reflective Pure Cu for Its High-Quality Additive Manufacturing, Adv. Eng. Mater. (2021) 2101138. https://doi.org/10.1002/adem.202101138.
[23] E. Uhlmann, K. Vasy, Extended Qualification of CuCr1Zr for the LBM Process, in: World PM, 2018.
[24] C. Wallis, B. Buchmayr, Effect of heat treatments on microstructure and properties of CuCrZr produced by laser-powder bed fusion, Mater. Sci. Eng. A. 744 (2019) 215–223. https://doi.org/10.1016/j.msea.2018.12.017.
[25] B. Buchmayr, G. Panzl, A. Walzl, C. Wallis, Laser Powder Bed Fusion – Materials Issues and Optimized Processing Parameters for Tool steels, AlSiMg- and CuCrZr-Alloys, Adv. Eng. Mater. 19 (2017). https://doi.org/10.1002/adem.201600667.
[26] C. Salvan, L. Briottet, T. Baffie, L. Guetaz, C. Flament, CuCrZr alloy produced by laser powder bed fusion: Microstructure, nanoscale strengthening mechanisms, electrical and mechanical properties, Mater. Sci. Eng. A. 826 (2021) 141915. https://doi.org/10.1016/j.msea.2021.141915.
[27] AFNOR, Standard EN12420:2014 - Cuivre et alliages de cuivre - Pièces forgées., (2014).
[28] C. Drive, Ion beam etch rates and sputter yields, (2020). www.ionbeam.co.uk.
[29] R. Condotta, Coulabilité des poudres cohésives: mesures aux faibles contraintes, granulaires humides et application à une poudre industrielle., PhD Thesis, Institut National Polytechnique de Toulouse, 2005.
[30] B.V. Crist, Handbook of monochromatic XPS spectra, Wiley, Chichester ; New York, 2000.
[31] J.F. Moulder, W.F. Stickle, P.E. Sobol, K.D. Bomben, Handbook of X-ray Photoelectron Spectroscopy, Perkin-Elmer Corporation, 1992.
[32] R.P. Vasquez, Cu2O by XPS, Surf. Sci. Spectra. 5 (1998) 257–261. https://doi.org/10.1116/1.1247881.
[33] R.P. Vasquez, CuCO3 by XPS, Surf. Sci. Spectra. 5 (1998) 273–278. https://doi.org/10.1116/1.1247884.
[34] R.P. Vasquez, Cu(OH)2 by XPS, Surf. Sci. Spectra. 5 (1998) 267–272. https://doi.org/10.1116/1.1247883.
[35] M.P. Seah, Pure element sputtering yields using 500–1000 eV argon ions, Thin Solid Films. 81 (1981) 279–287. https://doi.org/10.1016/0040-6090(81)90490-9.
[36] D. Barreca, G.A. Battiston, R. Gerbasi, E. Tondello, P. Zanella, Zirconium Dioxide Thin Films Characterized by XPS, Surf. Sci. Spectra. 7 (2000) 303–309. https://doi.org/10.1116/1.1375573.
[37] J.A. Treverton, N.C. Davies, XPS studies of a ferricyanide accelerated chromate paint pretreatment film on an aluminium surface, Surf. Interface Anal. 3 (1981) 194–200. https://doi.org/10.1002/sia.740030503.
[38] I. Ikemoto, K. Ishii, S. Kinoshita, X-Ray Photoelectron Spectroscopic Studies of CrOz and Some Related Chromium Compounds, (1976) 6.

[39] C. Battistoni, J.L. Dormann, D. Fiorani, E. Paparazzo, S. Viticoli, An XPS and Mössbauer study of the electronic properties of ZnCrxGa2−xO4 spinel solid solutions, Solid State Commun. 39 (1981) 581–585. https://doi.org/10.1016/0038-1098(81)90326-4.
[40] R.N. Caron, Copper: Alloying, in: Ref. Module Mater. Sci. Mater. Eng., Elsevier, 2016: p. B9780128035818025000. https://doi.org/10.1016/B978-0-12-803581-8.02563-7.
[41] I. Yadroitsev, Selective laser melting: direct manufacturing of 3D-objects by selective laser melting of metal powders, Lambert Acad. Publ, Saarbrücken, 2009.
[42] N&K Database, ANGSTROM SUN Technol. INC. (2022). http://www.angstec.com/graph/29.
[43] D. Bergström, The Absorption of Laser Light by Rough Metal Surfaces, 2008.